JOURNAL OF GEOPHYSICAL RESEARCH, VOL. 115, B06303, doi:10.1029/2009JB006884, 2010

Tsunami waveform inversion including dispersive waves: the 2004 earthquake off Kii Peninsula, Japan

Tatsuhiko Saito,[1] Kenji Satake,[2] and Takashi Furumura[2,3]

Received 16 August 2009; revised 23 December 2009; accepted 5 January 2010; published 3 June 2010.

[1] Long waves are often assumed to model tsunamis, but the wavelength of the initial water height distribution produced by a large submarine earthquake, particularly in the direction perpendicular to the fault strike, is sometimes not much greater than the water depth. The resulting tsunami may have a dispersive character that cannot be simulated based on a conventional long-wave approximation. The 2004 earthquake off Kii Peninsula (*M* 7.4) on the southern coast of Japan indeed produced a dispersive tsunami that was recorded at two stations located off Shikoku. For the foreshock (*M* 7.1), on the contrary, a dominant dispersive tsunami was not recognized at these stations. Because dispersive waves show strong directional dependence with respect to the fault strike, the above difference indicates that the strikes of the main shock and the foreshock were different. We conducted a tsunami waveform inversion analysis based on the dispersive tsunami equations to estimate the initial water height distribution of the main shock. The estimated initial water height distribution overlapped with the aftershock region, suggesting that the fault strike was perpendicular to the trough axis, and the total displaced water volume was 1.7–2.0 × 10^9 m^3. When we used the conventional long-wave approximation, the estimated initial water height distribution extended considerably from the aftershock area, because artificial sources were needed outside the aftershock area to reproduce the observed dispersive waves.

Citation: Saito, T., K. Satake, and T. Furumura (2010), Tsunami waveform inversion including dispersive waves: the 2004 earthquake off Kii Peninsula, Japan, *J. Geophys. Res.*, *115*, B06303, doi:10.1029/2009JB006884.

1. Introduction

[2] Tsunami waveform inversion analysis has been considered a powerful tool for estimating the seismic source process, and numerous studies have been done [e.g., *Satake*, 1989; *Fujii and Satake*, 2007; *Piatanesi and Lorito*, 2007]. One of the advantages of tsunami waveform analysis is that the path effects for tsunami propagation are expected to be correctly evaluated since the bathymetry is much better known than the seismic velocity structure. Also, it provides an estimate of the seismic source process independently from seismogram analysis, enabling us to check the accuracy and reliability of those results by comparison or to discuss differences in tsunami and seismic sources, such as in the case of a tsunami earthquake [*Kanamori*, 1972].

[3] The current tsunami waveform analysis method, however, has a few limitations. The major one is the use of linear long-wave (LLW) equations for simulating tsunami propagation. The long-wave approximation breaks down when the wavelength of the water height distribution is not much greater than the water depth. For intraplate earthquakes characterized by large dip angles whose initial water height distribution is composed of rich short-wavelength components, LLW equations cannot properly simulate dispersive tsunami propagation [*Saito and Furumura*, 2009a]. To overcome this limitation, we use the recently available powerful computers to solve alternative tsunami equations. Clusters of personal computers and supercomputers enable tsunami to be simulated very accurately in three-dimensional (3-D) space based on Navier-Stokes equations [e.g., *Furumura and Saito*, 2009]. In the meantime, numerical simulations of 2-D dispersive (DSP) tsunami equations have also been conducted on high-performance computers and personal computers in recent years [e.g., *Tanioka*, 2000; *Shigihara and Fujima*, 2006; *Horrillo et al.*, 2006]. The 2-D DSP tsunami equations, which are more efficient than 3-D simulation in terms of computational time, can correctly reproduce the 3-D simulation results for offshore tsunami records [*Saito and Furumura*, 2009a].

[4] Offshore tsunami records are now available, owing to the development of bottom-pressure gauges [e.g., *Baba et al.*, 2004] and real-time kinematic GPS techniques [*Kato et al.*, 2000]. Bottom-pressure gauges located in deep ocean bottoms (water depth >1000 m) can record dispersive tsunamis very clearly [*Matsumoto and Mikada*, 2005].

[1]National Research Institute for Earth Science and Disaster Prevention, Tsukuba, Japan.
[2]Earthquake Research Institute, University of Tokyo, Tokyo, Japan.
[3]Also at Center for Integrated Disaster Information Research, Interfaculty Graduate School of Interdisciplinary Information Studies, University of Tokyo, Tokyo, Japan.

0148-0227/10/2009JB006884

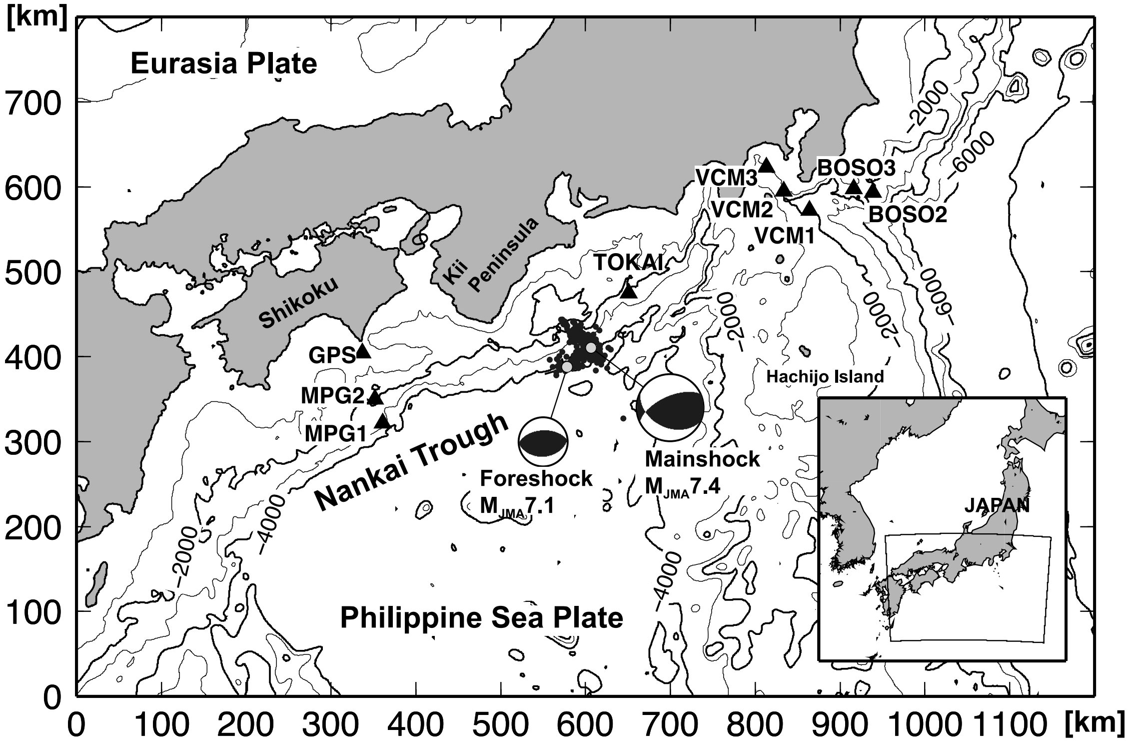

Figure 1. Bathymetry around Kii Peninsula, Japan. The water depth is contoured at intervals of 1000 m. The centroid moment tensor solutions for the 2004 earthquake off Kii Peninsula or the main shock (*M* 7.4, 1457 UTC) and its foreshock (*M* 7.1, 1007 UTC) determined by the National Research Institute for Earth Science and Disaster Prevention (NIED) [*Fukuyama et al.*, 1998] are plotted together with the epicenters of the aftershocks (filled circles) located by the Japan Meteorological Agency. Locations of the nine offshore tsunami gauges used in this study are indicated by filled triangles.

[5] Using DSP tsunami equations, the present study conducts a tsunami waveform inversion analysis to estimate the initial water height distribution of the 2004 earthquake off Kii Peninsula, Japan (the magnitude determined by the Japan Meteorological Agency is M_{JMA} 7.4). In particular, we take advantage of the analysis of dispersive waves, which contain important information about the fault strike. In this paper we first show the tsunami waveform data for the 2004 earthquake off Kii Peninsula recorded at offshore stations. We next explain the tsunami simulation based on DSP tsunami equations by comparing the results with those obtained with the nondispersive tsunami equations used in most conventional studies. We then conduct a tsunami waveform inversion analysis for the tsunami source of the 2004 earthquake off Kii Peninsula. The results of inversion are also compared with those derived using conventional nondispersive tsunami equations.

2. 2004 Earthquake Off Kii Peninsula (*M* 7.4)

[6] Along the Nankai trough, southwestern Japan, the Philippine Sea Plate is subducting underneath the Eurasian Plate (Figure 1). Great ($M \sim 8$) earthquakes have recurred along the fault between the two plates with a recurrence interval of the order of 100 years. The 1944 Tonankai (*M* 7.9) and the 1946 Nankai (*M* 8.0) earthquakes caused serious tsunami damage along the Pacific coast around this area. Numerous seismological investigations have been conducted to understand the tectonics around this megathrust-earthquake area. Slab segmentation is indicated by the seismic velocity structure and hypocentral distribution of small earthquakes including nonvolcanic tremors beneath the Kii Peninsula [e.g., *Shiomi and Park*, 2008; *Obara*, 2009]. *Miyoshi and Ishibashi* [2005] proposed a slab tearing in the Philippine Sea Plate; the tear, occurring from near trough, extends to beneath the Kii Peninsula with a NW-SE strike.

[7] A large earthquake (M_{JMA} 7.4, 1457 UTC) occurred off Kii Peninsula on 5 September 2004. Unlike the 1944 Tonankai and 1946 Nankai interplate events, this event was an intraplate event occurring in the outer rise of the Philippine Sea Plate. It was characterized as a reverse fault as shown by a centroid moment tensor solution (Figure 1). Many researchers have estimated the source mechanism or the slip distribution along the fault by analyzing the seismograms observed during this event [e.g., *Hara*, 2005; *Park and Mori*, 2005]. Y. Yamanaka proposed a fault model with a strike in the NW-SE direction (strike = 135°) by analysis of the far-field body waves (unpublished data available at ttp://www.eri.u-tokyo.ac.jp/sanchu/Seismo_Note/2004/EIC153.html). The fault direction is perpendicular to the trough axis and is consistent with the idea of a slab tearing in the Philippine Sea Plate [*Miyoshi and Ishibashi*, 2005]. On

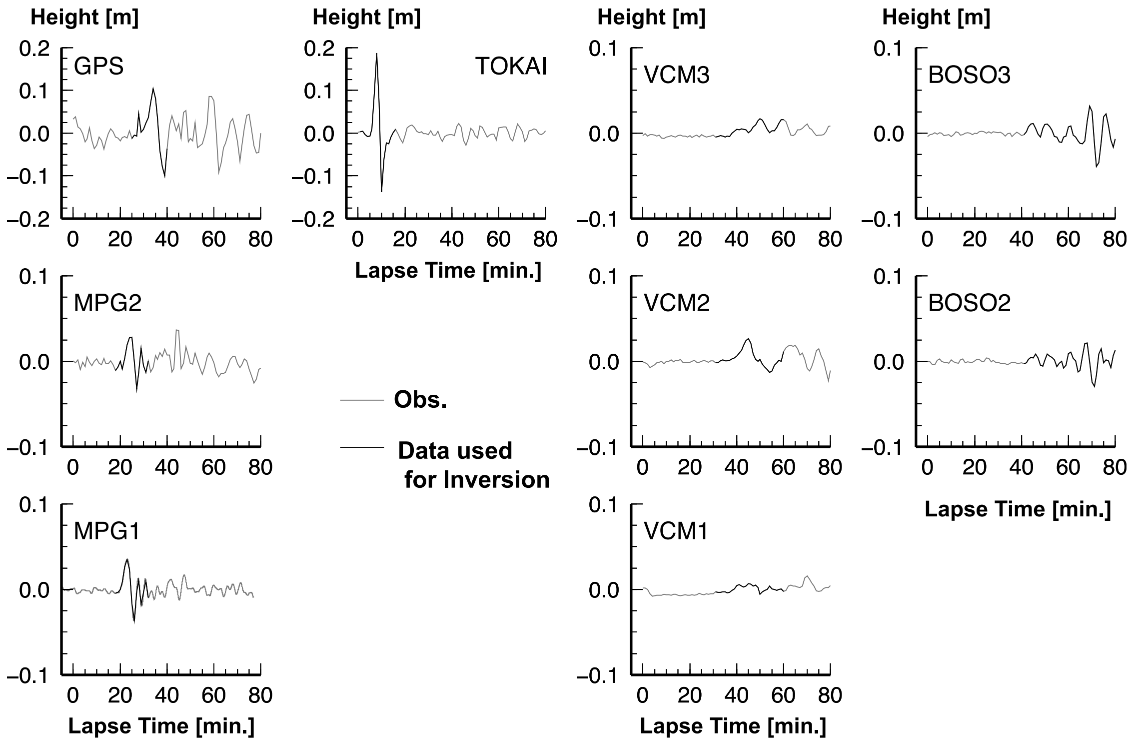

Figure 2. Offshore tsunami records for the 2004 earthquake off Kii Peninsula (gray (lighter) portions of lines). The black (darker) portions of the lines are used in the inversion analysis.

the contrary, different fault models with different fault strikes have been proposed by other researchers [e.g., *Ito et al.*, 2005; *Park and Mori*, 2005]. The aftershocks were distributed in both the NW-SE and the NEE-SWW directions for this event (Figure 1), which made it difficult to determine the fault plane and the fault strike. Agreement has not yet been reached as to the actual fault geometry, in particular, for the strike of the main shock, NW-SE or NEE-SWW. For the foreshock, however, there seems to be a consensus about the strike. The foreshock (M_{JMA} 7.1) occurred at 1007:08 (UTC) within the subducting Philippine Sea Plate. It was characterized by dip slip and a NEE-SWW fault strike (parallel to the trough axis) [*Ito et al.*, 2005: *Park and Mori*, 2005; Y. Yamanaka, unpublished data, 2004].

3. Data

[8] The tsunami from the main shock was recorded at nine offshore tsunami gauges [*Satake et al.*, 2005]; the locations are indicated by triangles in Figure 1. Eight stations, MPG1, MPG2, TOKAI, VCM1, VCM2, VCM3, BOSO2, and BOSO3, employ a bottom-pressure gauge to detect water height variation [e.g., *Hirata and Baba*, 2006], and one station, GPS, employs a real-time kinetic GPS system on a buoy [*Kato et al.*, 2000]. When large earthquakes occur these offshore stations can be used to detect offshore tsunami and issue a tsunami warning before it arrives at the coastline [e.g., *Tsushima et al.*, 2009]. In addition, the records are suitable for reliable estimation of the tsunami source because they are free from strong local-site effects inside a bay or if there is very shallow bathymetry. To retrieve the tsunami signals from the original records, we follow a filtering method employed by *Satake et al.* [2005]. Initially, a low-pass filter with a corner frequency of 2 min is applied for removal of the short-period wind and seismic noise. We then approximate the tidal component by fitting a polynomial function of order 5 and remove the tides from the record.

[9] Figure 2 shows the nine tsunami records retrieved from the original records. We obtained a fairly good signal-to-noise ratio for all nine records. The dominant period of the leading tsunami waves was approximately 5 min. A maximum amplitude of 20 cm was obtained at the TOKAI station, located approximately 100 km distant from the epicenter of the event. The GPS station deployed near the coast observed an amplitude of approximately 10 cm, and the other offshore stations observed an amplitude of a few centimeters. Two stations off Shikoku, MPG1 and MPG2, indicated a dispersive character, following peaks of ~3 cm amplitude [e.g., *Saito and Furumura*, 2009a]. For the foreshock (Figure 3), on the contrary, we did not recognize clear dispersive waves from those stations. Also, the maximum height arrived approximately 3 min earlier than that of the main shock. Considering that the source locations were almost identical between the foreshock and the main shock, we guess that the differences in waveforms between the foreshock and the main shock were caused mainly by differences in the source mechanisms rather than the difference in the paths. Hence we expect that analysis of the waveforms including those dispersive

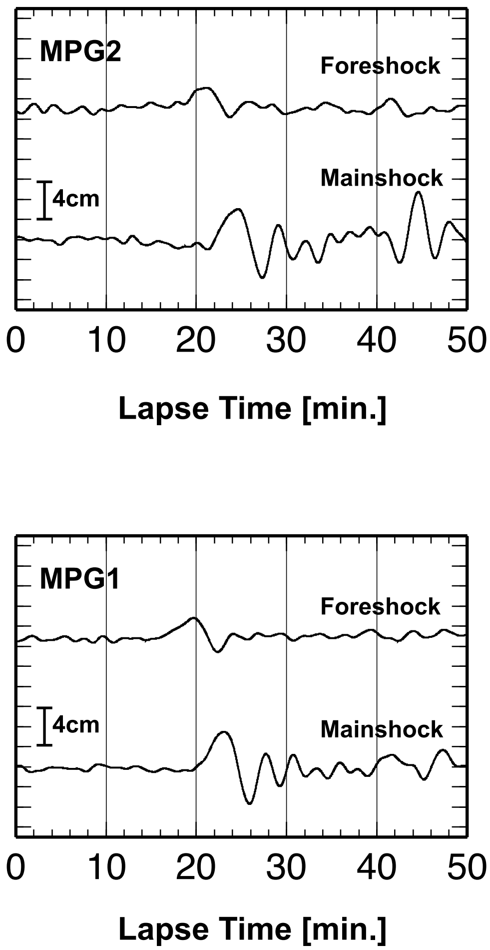

Figure 3. Tsunami waveforms of the foreshock and the main shock recorded at the two stations located off Shikoku (MPG1 and MPG2).

waves can provide us with essential information about the main shock source.

4. Dispersive (DSP) Tsunami Equations

[10] The 2-D linear DSP equations in the x-y coordinates are derived from the 3-D equations of motion of water waves as

$$\begin{aligned} \frac{\partial M}{\partial t} + gh\frac{\partial \eta}{\partial x} &= \frac{1}{3}h^2\frac{\partial^2}{\partial x \partial t}\left(\frac{\partial M}{\partial x} + \frac{\partial N}{\partial y}\right), \\ \frac{\partial N}{\partial t} + gh\frac{\partial \eta}{\partial y} &= \frac{1}{3}h^2\frac{\partial^2}{\partial y \partial t}\left(\frac{\partial M}{\partial x} + \frac{\partial N}{\partial y}\right), \\ \frac{\partial \eta}{\partial t} &= -\frac{\partial M}{\partial x} - \frac{\partial N}{\partial y} \end{aligned} \tag{1}$$

[e.g., *Peregrine*, 1972; *Saito and Furumura*, 2009a]. The parameters M and N are the velocity components integrated along the vertical direction from the sea bottom to the sea surface, η is the water height from the sea surface at rest, h is the water depth, and g is the gravitational constant. To solve these equations we employ an implicit scheme for finite-difference simulation (Appendix A). The right-hand sides of the first two equations (1) indicate dispersion terms. Neglecting the dispersion terms, we obtain the LLW equations as

$$\begin{aligned} \frac{\partial M}{\partial t} + gh\frac{\partial \eta}{\partial x} &= 0, \\ \frac{\partial N}{\partial t} + gh\frac{\partial \eta}{\partial y} &= 0, \\ \frac{\partial \eta}{\partial t} &= -\frac{\partial M}{\partial x} - \frac{\partial N}{\partial y}. \end{aligned} \tag{2}$$

Numerous studies on tsunami waveform inversion employ nondispersive LLW equations.

[11] We numerically solve these tsunami equations (equations (1) or (2)) in the target area region of 1200 × 800 km^2 (Figure 1) based on the finite-difference method using a grid spacing of 1 km and a time step of 1 s. Examples of the simulation results based on DSP (equations (1)) and nondispersive (equations (2)) tsunami equations are provided in Appendix B.

5. Inversion Method

[12] We estimate the initial water height distribution by inversion analysis of the tsunami waveforms. Taking the possible source area as a square of 200 × 200 km, we divide the region into 400 subregions with 10-km intervals (Figure 4). For each subregion the water height distribution

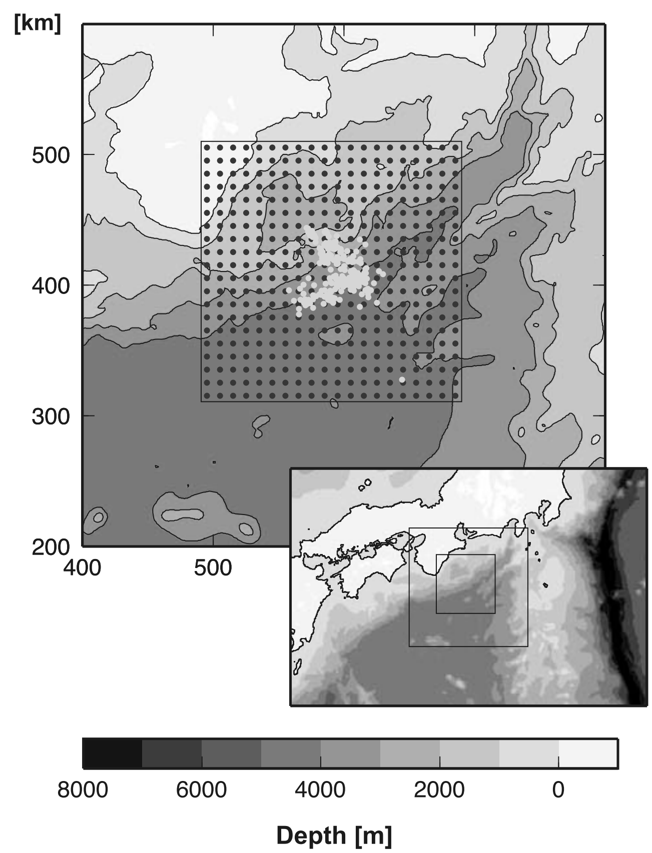

Figure 4. Distribution of basis functions for representing initial water height distribution (black (darker) filled circles). Epicenters of the aftershocks are plotted with gray (lighter) filled circles.

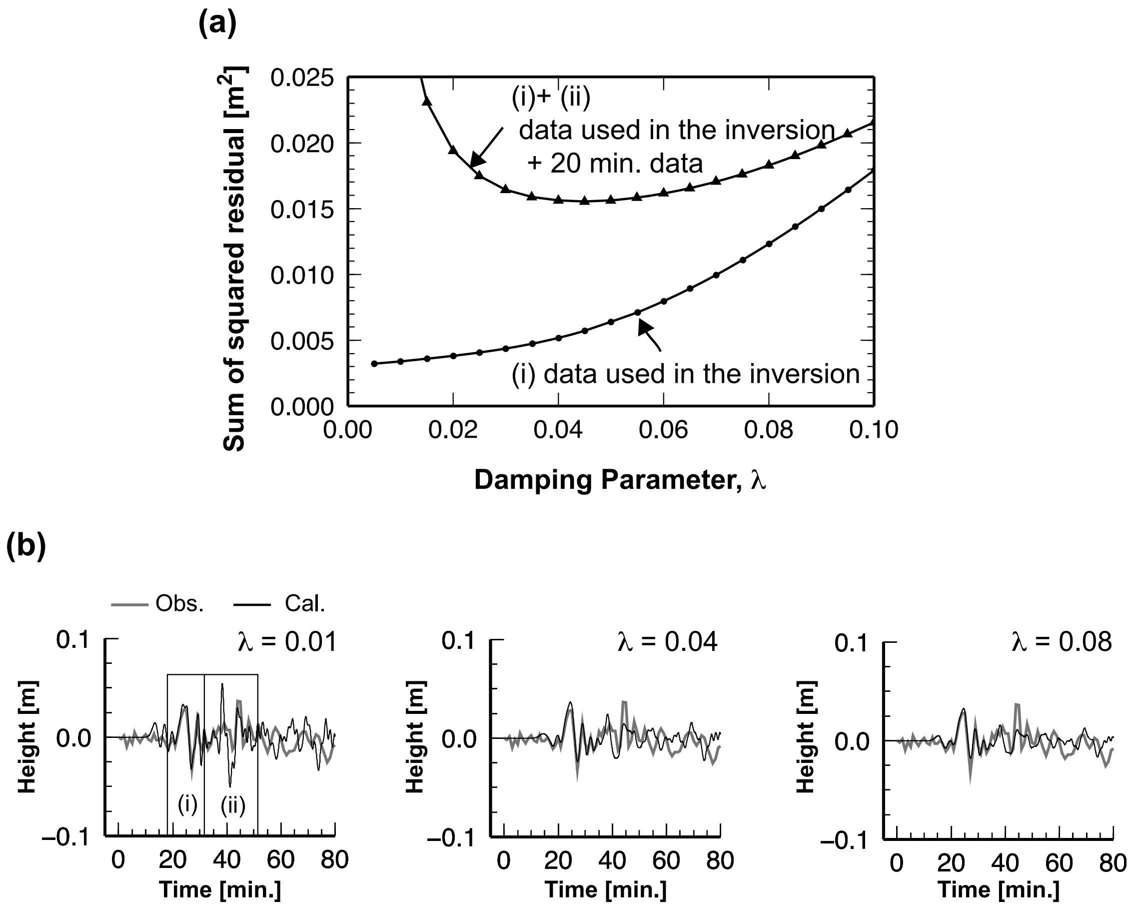

Figure 5. (a) Sum of the squared residuals for the data used in the inversion analysis (filled circles) and for the data used in the inversion analysis and additional 20 min data (filled triangles). (b) Comparisons of observed (gray (lighter) portions of lines) and calculated (black (darker) portions of lines) waveforms at TOKAI for damping parameter λ values of 0.01, 0.04, and 0.08.

is assumed to be given by the Gaussian function as a basis function,

$$\eta(x,y) = m_i \exp\left[-\frac{(x-x_i)^2 + (y-y_i)^2}{(L/2)^2}\right], \tag{3}$$

where the center of the ith subregion (i = 1, 2,…, 400) is located at (x_i, y_i). The spatial scale L is set to be 12 km in this study so as to reproduce realistic water height distributions around the source region, whose depth ranges between 2 and 4 km. This is based on the idea from linear potential theory (LPT) that the characteristic spatial scale of the initial water height distribution should be sufficiently large, that is, ~10 times greater than the water depth [*Saito and Furumura*, 2009b]. The height m_i is the model parameter to be estimated in the inversion analysis. We use the tsunami records as the data d_i in the inversion analysis (black portions of lines in Figure 2), which are the same as those used by *Satake et al.* [2005]. To obtain stable solutions the damped least-squares method is employed for the observational equation [e.g., *Aki and Richards*, 1980]:

$$\begin{pmatrix} \mathbf{d} \\ 0 \end{pmatrix} = \begin{pmatrix} \mathbf{A} \\ \lambda\mathbf{I} \end{pmatrix}\mathbf{m}. \tag{4}$$

The damped least-squares method provides a smoother solution in compensation for a larger residual between the observed and the calculated waveforms. In general, the larger the damping parameter λ, the smoother the solution but the worse the waveform fit. *Baba et al.* [2005] employed a similar method for inverting the model parameters of the tsunami source. They selected the damping parameter in such a way as to obtain a smooth solution consistent with the assumption of LLW theory or the long-wave approximation. This study does not assume the long-wave approximation. We hence selected an appropriate value for the damping parameter λ as follows. Figure 5a shows the sum of the squared residuals versus the damping parameter λ. The sum of the squared residuals for the data used in the inversion analysis (plotted with filled circles) takes its minimum value for λ = 0 (no damping) but increases with increasing values of λ. On the contrary, when we include the waveform for an additional 20 min in the sum of the squared residuals, the sum of the squared residual (plotted with filled triangles) takes its minimum value when the value of λ is 0.04. Figure 5b compares the observed waveforms and the calculated waveforms for various values of λ. A λ value of 0.01 is too small for damping, so the calculated waveform overestimates the amplitude of the later

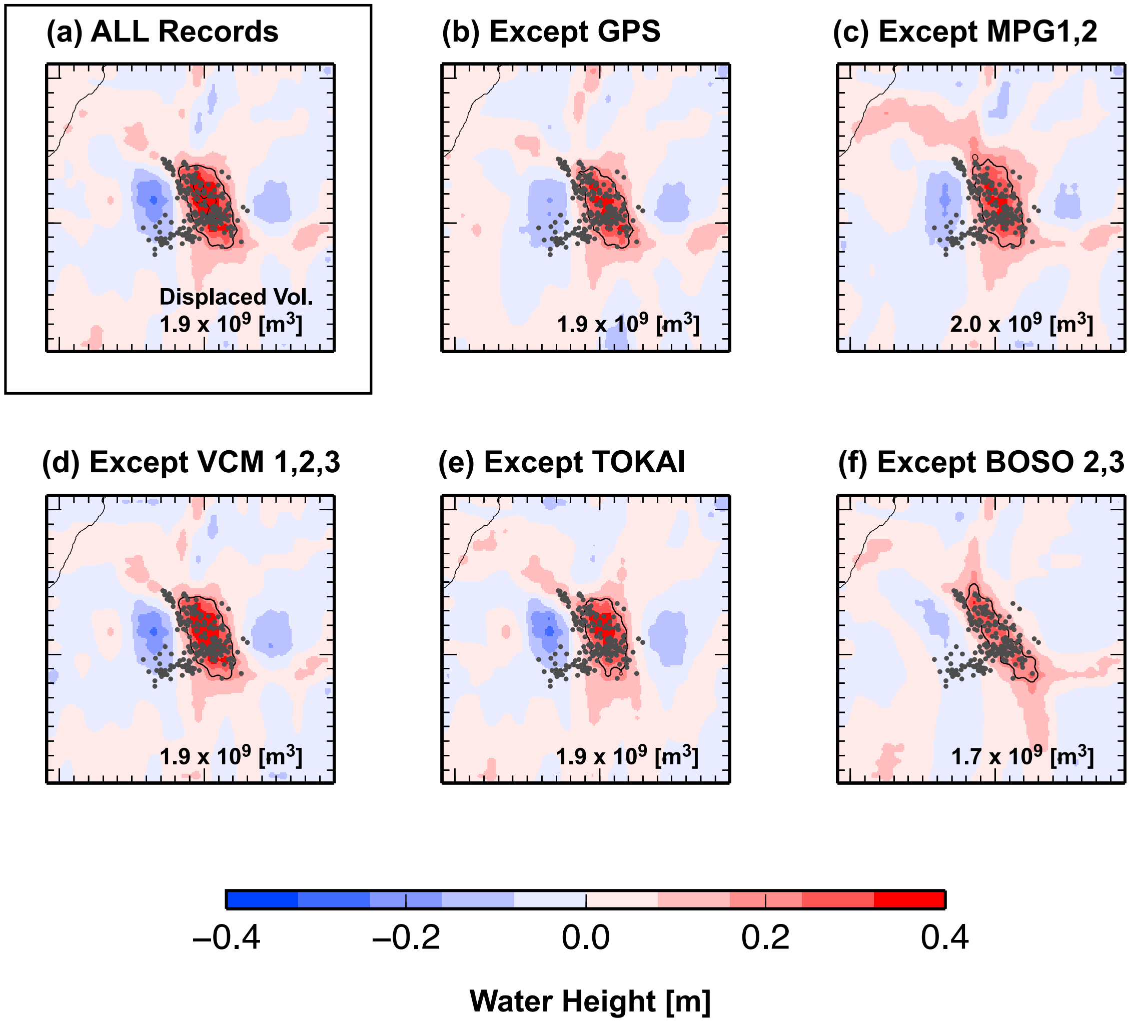

Figure 6. Initial water height distribution estimated based on the dispersive tsunami equations (a) using all nine tsunami records, (b) without GPS, (c) without MPG1 and MPG2, (d) without VCM1, VCM2, and VCM3, (e) without TOKAI, and (f) without BOSO2 and BOSO3.

waves. A λ value of 0.08 is too large for damping, so the calculated waveform underestimates the amplitude of the leading wave. A value of λ = 0.04 is a suitable damping parameter in this case; it reproduces both the leading wave and the later waves appropriately. We use the value of λ = 0.04 for the inversion analysis in this study. Computation of residuals for additional waveforms is a kind of validation test of the solution to examine how well the solution explains the data not used for the inversion.

6. Results

6.1. Initial Water Height Distribution

[13] Figure 6a shows the initial water height distribution calculated from the model parameters estimated by the inversion analysis. The result clearly suggests that the seismic fault exciting the tsunami is striking NW-SE (perpendicular to the trench axis). The initial water height distribution overlaps with the aftershock region extending in the NW-SE direction. Figure 7 compares the observed waveforms with the calculated waveforms. The calculated waveforms reproduce accurately the observed waveforms for the data used in the inversion analysis. Furthermore, for stations GPS, MPG1, MPG2, and TOKAI, the calculated waveforms roughly reproduce the waveform, or its envelopes, even after the data used in the inversion analysis.

[14] To examine the robustness of the estimated initial water height distribution, we then conducted an inversion analysis excluding some of the tsunami records and estimated the initial water height distribution. Figures 6b–6f show the initial water height distribution estimated without using stations GPS (Figure 6b), MPG1 and MPG2 (Figure 6c), VCM1, VCM2, and VCM3 (Figure 6d), TOKAI (Figure 6e), and BOSO2 and BOSO3 (Figure 6f), respectively. The area in which the water height is >0.2 m (outlined by solid curves in Figure 6) is stable, irrespective of the data used in the inversion analysis. When MPG1 and MPG2 were excluded from the inversion analysis (Figure 6c), the uplifted area extended considerably from the aftershock region. This indicates that the records of MPG1 and MPG2 contributed to the stable resolution for the estimation of the water height distribution. When BOSO2

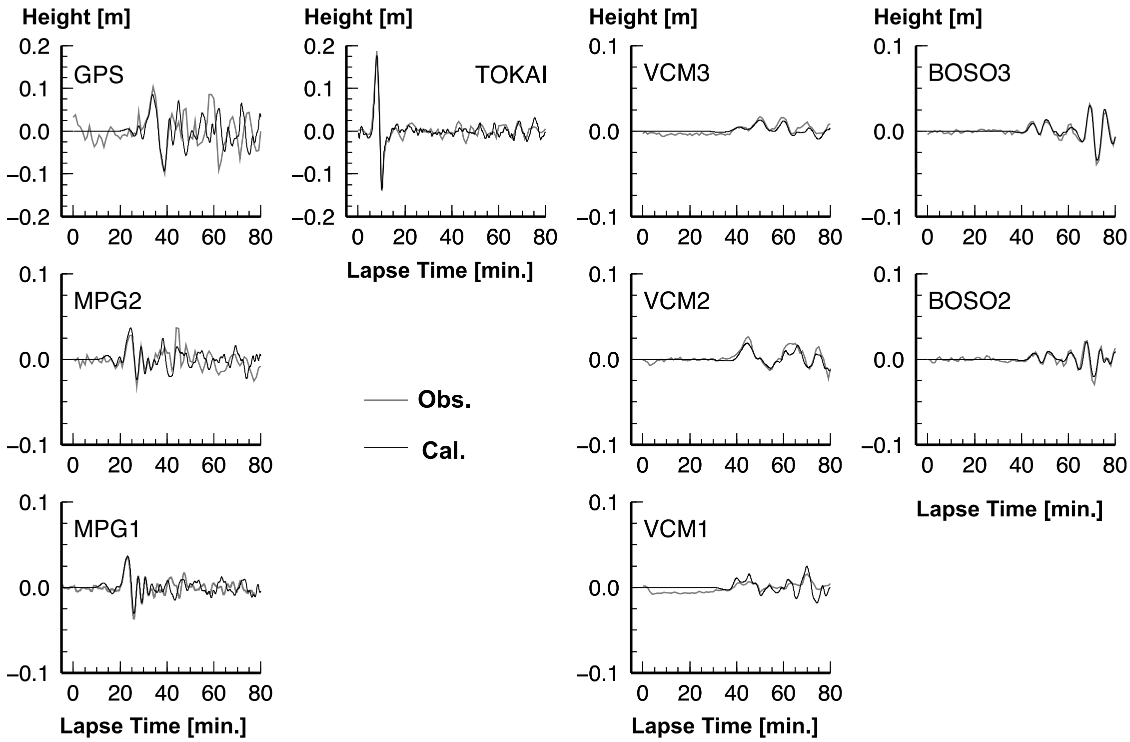

Figure 7. Comparison of the observed (obs.) and calculated (cal.) waveforms, based on the dispersive equations using the initial water height distribution in Figure 6a.

and BOSO3 were excluded from the inversion analysis (Figure 6f), the area with a water height >0.2 m was slightly different from the others. This difference was due to high-amplitude waves scattered from Hachijo Island and arriving at an elapsed time of >60 min in BOSO2 and BOSO3 (Figure 7). Even though slight differences between Figure 6c and Figure 6f can be recognized, for all cases (Figures 6a–6f), the uplifted area corresponded well to the aftershock region extending in the NW-SE direction. This feature can also be recognized in the initial water height distributions of *Baba et al.* [2005] and *Satake et al.* [2005]. However, note that the correspondence between the uplifted area and the aftershock region in our estimation is better than in these past studies. The estimated total amount of displaced water volume ranged between 1.7×10^9 and 2.0×10^9 m^3.

6.2. Comparison of Results Based on DSP Versus Nondispersive Equations

[15] To examine the differences between DSP and nondispersive LLW equations for the case of the 2004 Kii event, Figure 8 compares the simulation results on tsunami propagation from the estimated initial water height distribution (Figure 6a) based on DSP and LLW equations. The LLW simulation results were almost the same as those of the DSP simulations for all stations except MPG1 and MPG2. However, the MPG1 and MPG2 records calculated based on LLW equations overestimated the maximum amplitude and failed to simulate the following phases. The LLW equations failed to simulate tsunami dispersion for MPG1 and MPG2, which were located in the direction perpendicular to the fault strike.

[16] We then conducted an inversion analysis based on the LLW equations. The procedure for the inversion analysis was the same as that in the previous section, but we used LLW equations to simulate tsunami propagation. Figures 9a and 9b show the initial water height distribution estimated based on DSP and LLW equations. The initial water height distribution estimated using the LLW equations (Figure 9b) extended considerably from the aftershock region. To reproduce the dispersive tsunami in the observed records, artificial tsunami sources had to be located outside the aftershock region when nondispersive tsunami equations were used. It should be noted that the calculated tsunami records from the initial water height distribution in Figure 9b based on the LLW equation were able to reproduce the observed records as accurately as when DSP equations were used. The values of the variance were 2.75×10^{-5} and 2.29×10^{-5} m^2 for the DSP and the LLW equations, respectively. Using the LLW equations results in a smaller variance, but the dispersive waves cannot be simulated properly; the dispersive waves have to be simulated as waves from artificial sources. This indicates that we cannot judge the validity of the inversion results by considering only the residuals between observations and calculations, particularly when large numbers of model parameters are used and damping is applied in the inversion. The total amount of displaced water volume was estimated as 2.0×10^9 m^3 when we used LLW equations. This value was equivalent to the estimation obtained with the DSP tsunami equations, taking the error range into account.

6.3. Seismic Moment

[17] The result of our inversion (Figure 6a) indicates that the 2004 event off Kii Peninsula was mainly characterized

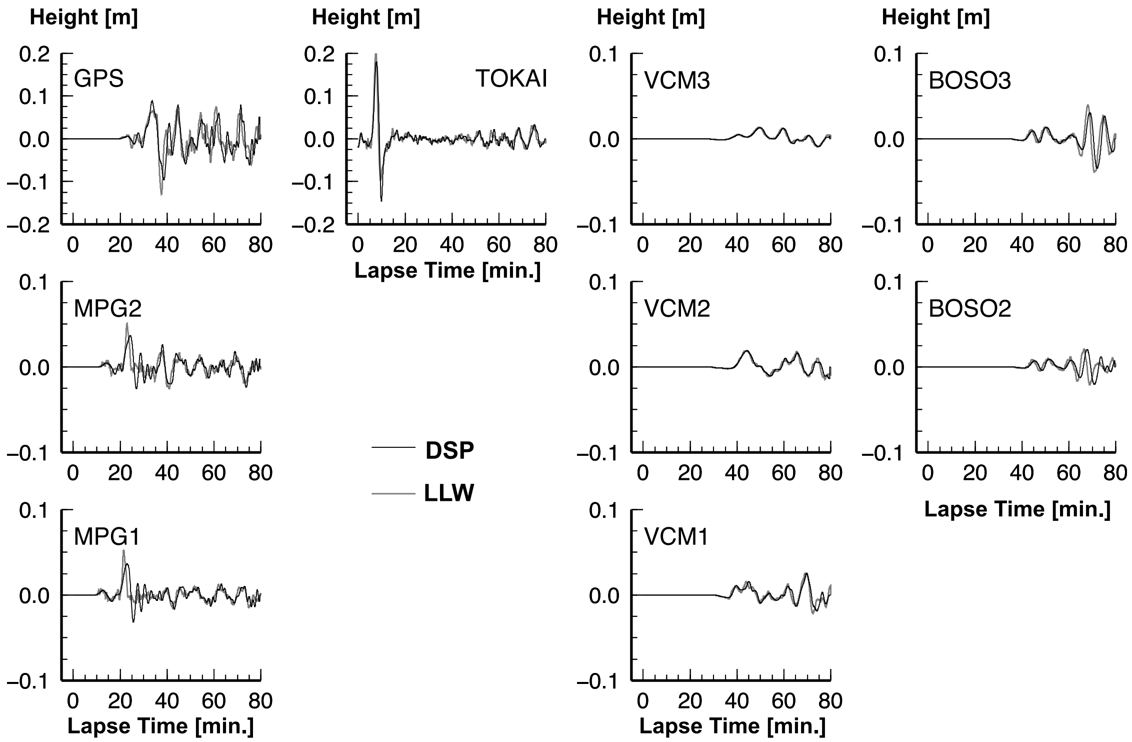

Figure 8. Comparisons of the calculated waveforms based on the dispersive (DSP) equations and the linear long-wave (LLW) equations. The waveforms are calculated with the common initial water height distribution (Figure 6a).

by the fault plane striking NW-SE. Employing the fault model striking in the NW-SE direction proposed from the teleseismic waveform analysis by Y. Yamanaka (unpublished data available at http://www.eri.u-tokyo.ac.jp/sanchu/Seismo_Note/2004/EIC153.html), we then estimated the fault slip and the seismic moment from the tsunami waveform. The fault plane, which was 70 km long and 32 km wide, was characterized by a strike of 135°, a dip of 40°, and a rake of 123°. The top depth of the fault was 2.3 km. We calculated the sea-bottom deformation with

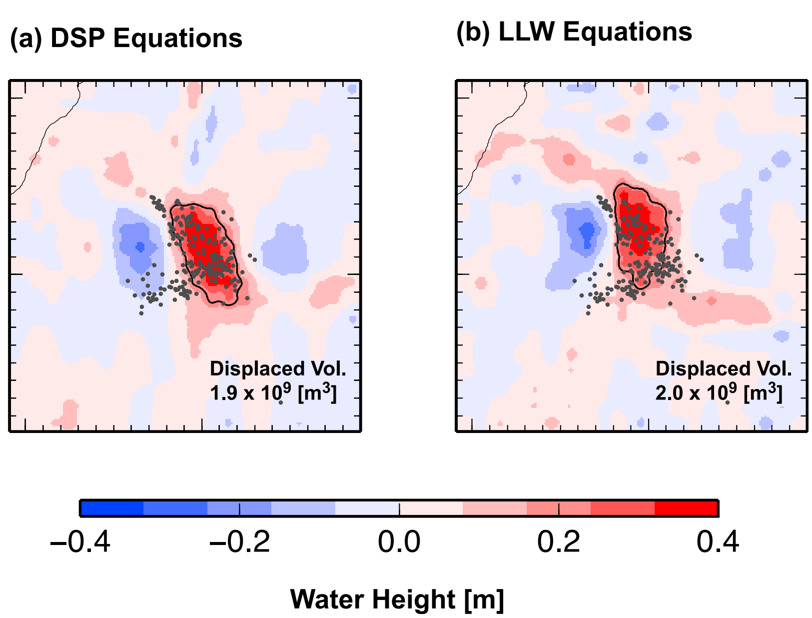

Figure 9. Comparison of the initial water height distribution estimated based on (a) DSP equations and (b) LLW equations. Black lines outline the area where the water height is >0.2 m. The total displaced water volume is also listed at the lower right in each plot.

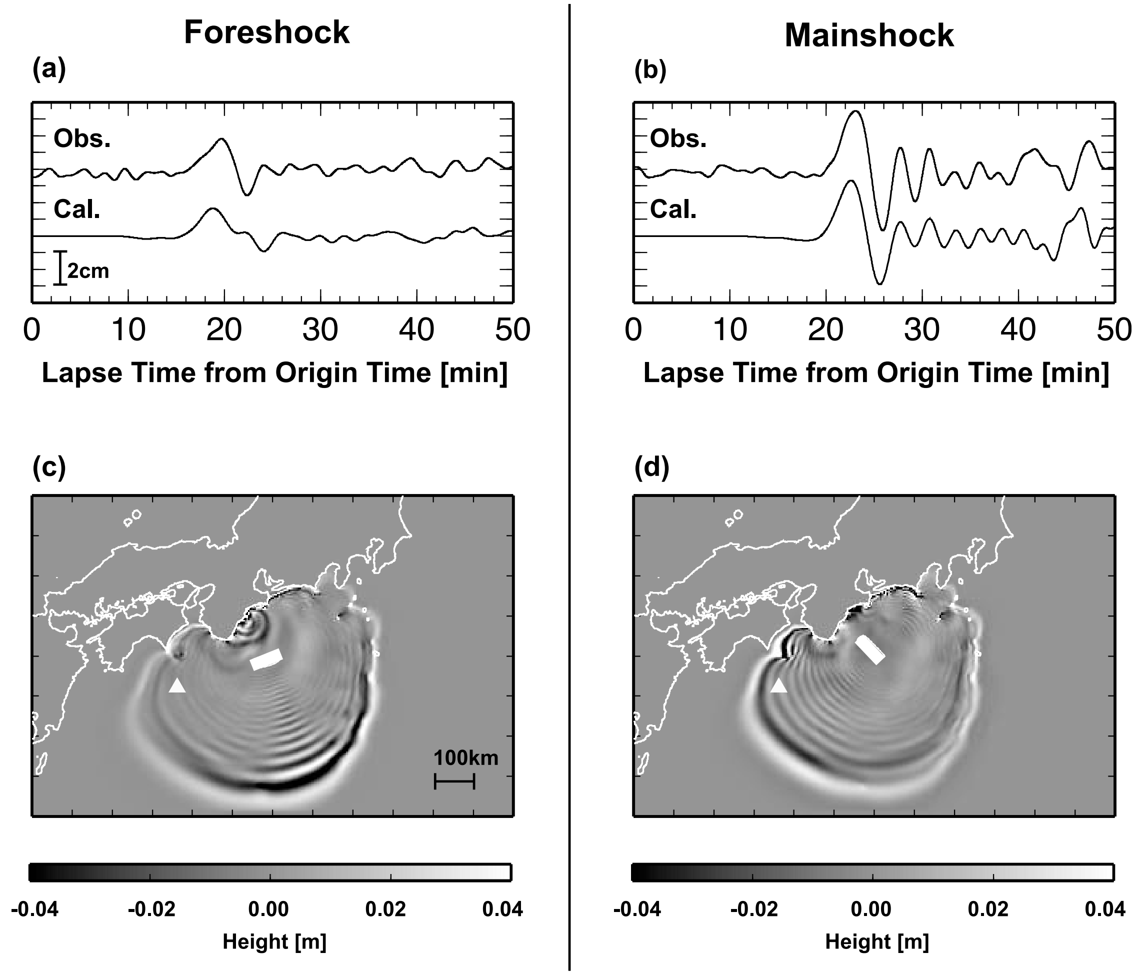

Figure 10. Comparison of the tsunami propagation for the foreshock (*M* 7.1, 1007 UTC) and the main shock (*M* 7.4, 1457 UTC). Tsunami waveforms were recorded and calculated at MPG1 for (a) the foreshock and (b) the main shock. Snapshots of the tsunami simulation were taken at an elapsed time of 30 min for (c) the foreshock and (d) the main shock. Triangles indicate the location of MPG1. Rectangles indicate the source region of the foreshock and the main shock.

the fault model assuming a homogeneous subsurface structure [*Okada*, 1985] and calculated the water height distribution from the sea-bottom deformation assuming a constant water depth of 2 km [*Takahashi*, 1942; *Saito and Furumura*, 2009b]. The tsunami propagation was numerically calculated on the basis of the DSP equations. From the tsunami waveform inversion the average slip on the fault was estimated as D = 1.32 m. When we used the same method for estimating robustness as was used for the initial water height distribution in Figure 6, the estimated slip ranged from 1.18 to 1.46 m. The seismic moment was estimated as $M_0 = 7.75 \times 10^{19}$ Nm when the upper crust structure of the preliminary reference Earth model (PREM) was used [*Dziewonski and Anderson*, 1981]. The estimated seismic moment ranged from 7.03×10^{19} to 8.70×10^{19} Nm, and the moment magnitude M_W ranged from 7.16 to 7.23.

6.4. Fault Strike and Dispersive Tsunamis

[18] The dispersive tsunami indicated a strong directional dependence with respect to the fault strike (Figure B1a). By using this outstanding feature of the dispersion, this section compares the fault directions of the foreshock (M_{JMA} 7.1, 1007 UTC) and the main shock (M_{JMA} 7.4, 1457 UTC). Figure 10a indicates the observed and calculated tsunami records at MPG1 for the foreshock. In the calculation we used a source model of Y. Yamanaka, which had a NEE-SWW strike (parallel to the trench axis) (unpublished data available at ttp://www.eri.u-tokyo.ac.jp/sanchu/Seismo_Note/2004/EIC153.html). The observed tsunami record does not show dominant dispersive tsunamis following the leading wave, and the maximum tsunami height arrived approximately 20 min after the time of origin. These two features are well simulated by the fault model striking in the NEE-SWW direction. Figure 10c indicates the corresponding simulation result for the water height distribution at an elapsed time of 20 min after the time of origin. The dispersive tsunami developed efficiently toward the SSE direction from the source, whereas dispersion was weak toward MPG1. Figure 10b indicates the observed and calculated tsunami records at MPG1 for the main shock. In the calculation we

used a source model of Y. Yamanaka, which had a strike of NW-SE (perpendicular to the trench axis). This source model, which is consistent with our tsunami inversion analysis (Figure 6), simulated accurately the arrival time and the dispersive tsunamis observed at MPG1. Figure 10d indicates that the dispersive tsunami developed efficiently toward the MPG1 station. The preceding tsunami simulation results and observed records of the foreshock and the main shock strongly suggest that the fault direction of the main shock had a NW-SE strike, which is different from that of the foreshock.

7. Conclusion

[19] We conducted a tsunami waveform inversion analysis for estimation of the initial water height distribution of the 2004 earthquake off Kii Peninsula, Japan (*M* 7.4). The dispersive tsunami was observed at the stations located off Shikoku (MPG1 and MPG2) during this event, which is well simulated based on the DSP tsunami equations. On the contrary, for the foreshock (*M* 7.1) the dominant dispersive tsunami was not recognized at those stations. This suggests that the strikes of the faults were different between the main shock and the foreshock because dispersive waves have a strong directional dependence with respect to the fault strike. The result of the inversion analysis for the main shock indicates that the initial water height distribution overlapped with the aftershock region, suggesting that the fault had a NW-SE strike (perpendicular to the trench axis) and the total displaced water volume was between 1.7×10^9 and 2.0×10^9 m^3. On the contrary, the initial water height distribution estimated by using the conventional LLW equations extended considerably from the aftershock region. To reproduce the dispersive tsunami in the observed records, artificial tsunami sources had to be located outside the aftershock region when nondispersive equations were used. The total displaced water volume (2.0×10^9 m^3) was equivalent to the estimation using the DSP tsunami equation, when the error range was taken into account.

Appendix A: Finite-Difference Scheme for Linear DSP Equations

[20] Using finite differentiation with a grid size of Δx and Δy in space and Δt in time, the DSP tsunami equations (equation (1)) can be expressed in finite-difference form as

$$\eta_{i,j}^{n+1} = \eta_{i,j}^{n} - \frac{\Delta t}{\Delta x} M_{i+1,j}^{n+\frac{1}{2}} + \frac{\Delta t}{\Delta x} M_{i,j}^{n+\frac{1}{2}} - \frac{\Delta t}{\Delta y} N_{i,j+1}^{n+\frac{1}{2}} + \frac{\Delta t}{\Delta y} N_{i,j}^{n+\frac{1}{2}}, \quad \text{(A1)}$$

$$\begin{aligned} &- \frac{h_m^2}{3\Delta x^2} M_{i+1,j}^{n+\frac{1}{2}} + \left(1 + \frac{2h_m^2}{3\Delta x^2}\right) M_{i,j}^{n+\frac{1}{2}} - \frac{h_m^2}{3\Delta x^2} M_{i-1,j}^{n+\frac{1}{2}} - \frac{h_m^2}{3\Delta x \Delta y} N_{i,j+1}^{n+\frac{1}{2}} \\ &\quad + \frac{h_m^2}{3\Delta x \Delta y} N_{i-1,j+1}^{n+\frac{1}{2}} + \frac{h_m^2}{3\Delta x \Delta y} N_{i,j}^{n+\frac{1}{2}} - \frac{h_m^2}{3\Delta x \Delta y} N_{i-1,j}^{n+\frac{1}{2}} \\ &= M_{i,j}^{n-\frac{1}{2}} - g h_m \frac{\Delta t}{\Delta x}\left(\eta_{i,j}^{n} - \eta_{i-1,j}^{n}\right) - \frac{h_m^2}{3\Delta x^2}\left(M_{i+1,j}^{n-\frac{1}{2}} - 2M_{i,j}^{n-\frac{1}{2}} + M_{i-1,j}^{n-\frac{1}{2}}\right) \\ &\quad - \frac{h_m^2}{3\Delta x \Delta y}\left(N_{i,j+1}^{n-\frac{1}{2}} - N_{i-1,j+1}^{n-\frac{1}{2}} - N_{i,j}^{n-\frac{1}{2}} + N_{i-1,j}^{n-\frac{1}{2}}\right), \quad \text{(A2)} \end{aligned}$$

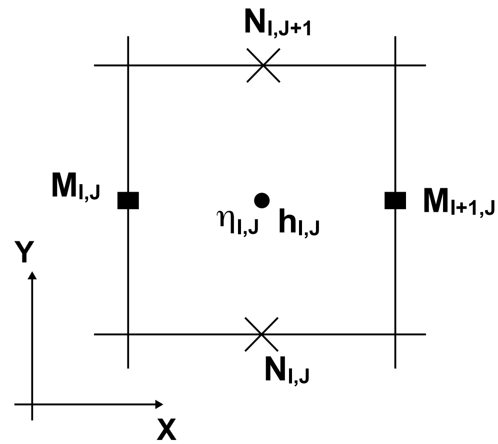

Figure A1. Staggered grids for the finite-difference simulation of linear dispersive equations.

$$\begin{aligned} &- \frac{h_n^2}{3\Delta y^2} N_{i,j+1}^{n+\frac{1}{2}} + \left(1 + \frac{2h_n^2}{3\Delta y^2}\right) N_{i,j}^{n+\frac{1}{2}} - \frac{h_n^2}{3\Delta y^2} N_{i,j-1}^{n+\frac{1}{2}} - \frac{h_n^2}{3\Delta x \Delta y} M_{i,j+1}^{n+\frac{1}{2}} \\ &\quad + \frac{h_n^2}{3\Delta x \Delta y} M_{i,j}^{n+\frac{1}{2}} + \frac{h_n^2}{3\Delta x \Delta y} M_{i+1,j-1}^{n+\frac{1}{2}} - \frac{h_n^2}{3\Delta x \Delta y} M_{i,j-1}^{n+\frac{1}{2}} \\ &= N_{i,j}^{n-\frac{1}{2}} - g h_n \frac{\Delta t}{\Delta y}\left(\eta_{i,j}^{n} - \eta_{i,j-1}^{n}\right) \\ &\quad - \frac{h_n^2}{3\Delta x \Delta y}\left(M_{i+1,j}^{n-\frac{1}{2}} - M_{i,j}^{n-\frac{1}{2}} - M_{i+1,j-1}^{n-\frac{1}{2}} + M_{i,j-1}^{n-\frac{1}{2}}\right) \\ &\quad - \frac{h_n^2}{3\Delta y^2}\left(N_{i,j+1}^{n-\frac{1}{2}} - 2N_{i,j}^{n-\frac{1}{2}} + N_{i,j-1}^{n-\frac{1}{2}}\right), \quad \text{(A3)} \end{aligned}$$

where the surface fluctuation $\eta_{i,j}^{n}$, water depth $h_{i,j}$, and integrated horizontal velocity components $M_{i,j}^{n+\frac{1}{2}}$ and $N_{i,j}^{n+\frac{1}{2}}$ are arranged in the staggered grids shown in Figure A1. The surface fluctuation is defined at time $t = n \cdot \Delta t$, and the integrated horizontal velocity components are defined at time $t = (n + 1/2)\Delta t$, where $n = 0, 1, 2, \ldots$. The depth of hm and hn are obtained by interpolation of the depth as $h_n = (h_{i,j} + h_{i,j-1})/2$ and $h_m = (h_{i,j} + h_{i-1,j})/2$, respectively. At time $t = n \times \Delta t$ we calculate $M_{i,j}^{n+\frac{1}{2}}$ and $N_{i,j}^{n+\frac{1}{2}}$ for the next time step of $t = (n + 1/2)\Delta t$ with an implicit scheme. By solving the linear system of equations (A2) and (A3) with an iterative method (Gauss-Seidel method) [e.g., *Press et al.*, 1986], we obtain $M_{i,j}^{n+\frac{1}{2}}$ and $N_{i,j}^{n+\frac{1}{2}}$. Substituting the obtained $M_{i,j}^{n+\frac{1}{2}}$ and $N_{i,j}^{n+\frac{1}{2}}$ into (A1), we then obtain the sea surface fluctuation $\eta_{i,j}^{n+1}$ for the next time step, $t = (n + 1)\Delta t$.

Appendix B: DSP and Nondispersive Tsunami Simulations

[21] We compare the simulation results based on the DSP equations (1) and the nondispersive LLW equations (2). Tsunami generation for a *M* 7.4 earthquake is considered based on a scaling law [*Kanamori and Anderson*, 1975]; the fault length L is 80 km, the fault width W is 40 km, the dislocation along the fault D is 1.6 m, and the moment M_0 is 1.37×10^{20} Nm (M_W 7.36). The dip angle is assumed to be 40°, and the top depth of the fault plane is assumed to

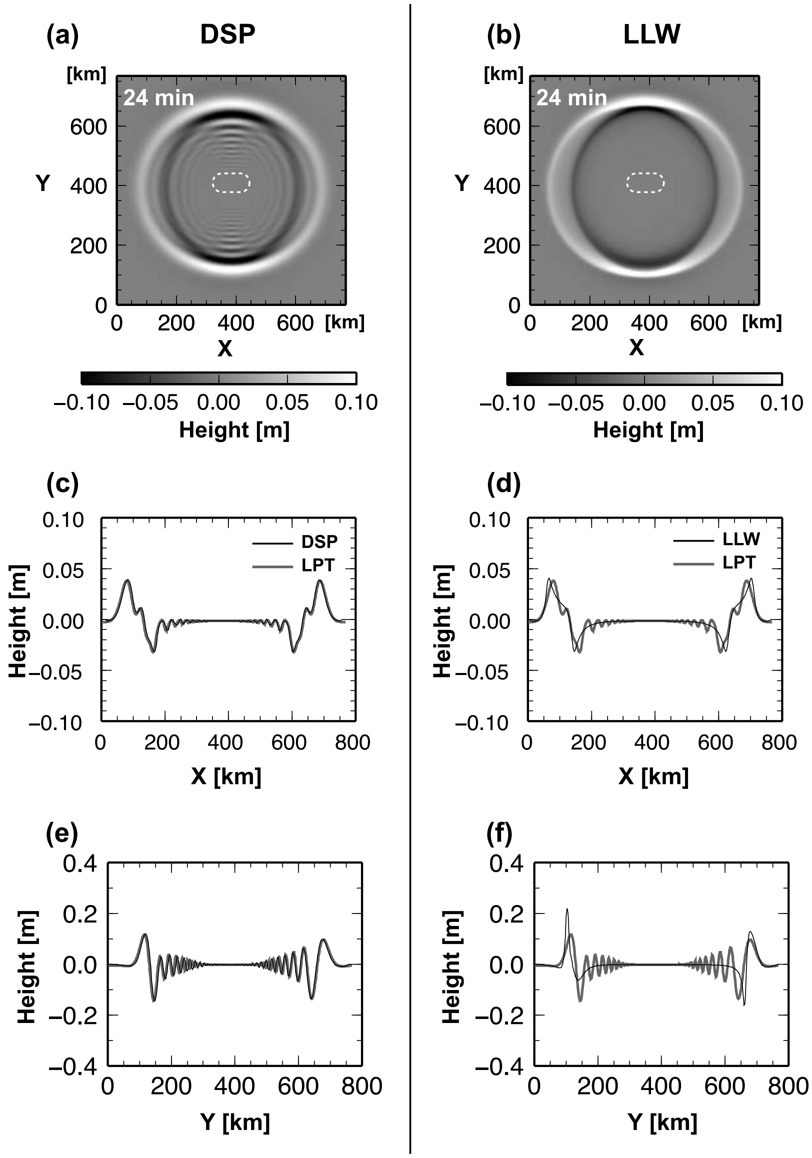

Figure B1. Snapshots of tsunami propagation (map view) at an elapsed time of 24 min after the earthquake origin time calculated by (a) DSP equations and (b) nondispersive LLW equations. Water height distribution along the axis parallel to the fault strike (Y = 384 km): (c) comparison of simulation results based on DSP equations versus linear potential theory (LPT) and (d) comparison of simulation results based on LLW equations versus LPT. Water height distribution along the axis perpendicular to the fault strike (X = 384 km): (e) comparison of simulation results based on DSP equations versus LPT and (f) comparison of simulation results based on LLW equations versus LPT.

be 4 km beneath the ocean floor. We calculate the vertical displacement at the sea bottom caused by the fault in the homogeneous half-space [*Okada*, 1985] and assume a sea-bottom deformation with a risetime T of 10 s and a constant sea depth of 4 km. We also calculate waveforms based on the analytical expression of LPT [e.g., *Takahashi*, 1942] for comparison. In the methods of DSP and LLW equations, we use equation (39) of *Kajiura* [1963] to calculate the initial water height distribution from the sea-bottom deformation.

[22] Figures B1a and B1b show the water height distribution at an elapsed time of 24 min after the earthquake origin time, calculated from the DSP and LLW equations, respectively. DSP equations generate the later phases, which are dispersive tsunamis, following the leading wave propagating along the y axis. The LLW equations, on the contrary, cannot simulate the dispersive waves (Figure B1b). Figures B1c and B1d show cross sections of the height distribution on the sea surface along the axis parallel to the fault strike (Y = 384 km in Figures B1a and B1b). The water height distribution calculated based on LPT is also plotted (gray lines) for comparison. These figures indicate that both DSP (Figure B1c) and LLW (Figure B1d) equations can roughly reproduce the height distribution calculated by LPT. On the contrary, in Figures B1e and

B1f, for the case of cross sections along the axis perpendicular to the fault strike ($X = 384$ km in Figures B1a and B1b), there is a large discrepancy in the results between LLW equations and LPT (Figure B1f). The LLW equations cannot simulate the later phases following the leading wave. A significant difference in the height of the leading wave is also recognized. These differences are due to the dispersion that is not included in the LLW equations. On the other hand, the DSP equations accurately reproduce the results of LPT for all elapsed times (Figure B1e).

[23] The above comparisons among DSP and LLW equations and LPT suggest that DSP equations are more appropriate to simulate tsunami waves, including the short-wavelength components.

[24] **Acknowledgments.** We used records from offshore tsunami gauges operated by the Japan Agency for Marine-Earth Science and Technology (JAMSTEC), the Japan Meteorological Agency (JMA), the Earthquake Research Institute, University of Tokyo (ERI), and the National Research Institute for Earth Science and Disaster Prevention (NIED), presented by *Satake et al.* [2005]. We thank anonymous reviewers for constructive comments. The GMT software package [*Wessel and Smith*, 1998] was used to construct the figures.

References

Aki, K., and P. G. Richards (1980), *Quantitative Seismology*, W. H. Freeman, San Francisco.

Baba, T., K. Hirata, and Y. Kaneda (2004), Tsunami magnitude determined from ocean-bottom pressure gauge data around Japan, *Geophys. Res. Lett.*, *31*, L08303, doi:10.1029/2003GL019397.

Baba, T., P. R. Cummins, and T. Hori (2005), Compound fault rupture during the 2004 off the Kii Peninsula earthquake (M 7.4) inferred from highly resolved coseismic sea-surface deformation, *Earth Planets Space*, *57*, 167–172.

Dziewonski, A. M., and D. L. Anderson (1981), Preliminary reference Earth model, *Phys. Earth Planet. Inter.*, *25*, 297–356, doi:10.1016/0031-9201(81)90046-7.

Fujii, Y., and K. Satake (2007), Tsunami source of the 2004 Sumatra-Andaman earthquake inferred from tide gauge and satellite data, *Bull. Seismol. Soc. Am.*, *97*, S192–S207, doi:10.1785/0120050613.

Fukuyama, E., M. Ishida, D. Dreger, and H. Kawai (1998), Automated seismic moment tensor determination by using on-line broadband seismic waveforms, *Zisin 2*, *51*, 149–156 (in Japanese with English abstract).

Furumura, T., and T. Saito (2009), Integrated ground motion and tsunami simulation for the 1944 Tonankai earthquake using high-performance supercomputers, *J. Disaster Res.*, *4*, 118–126.

Hara, T. (2005), Change of the source mechanism of the main shock of the 2004 off the Kii peninsula earthquakes inferred from long period body wave data, *Earth Planets Space*, *57*, 179–183.

Hirata, K., and T. Baba (2006), Transient thermal response in ocean bottom pressure measurement, *Geophys. Res. Lett.*, *33*, L10606, doi:10.1029/2006GL026084.

Horrillo, J., Z. Kowalik, and Y. Shigihara (2006), Wave dispersion study in the Indian Ocean-tsunami of December 26, 2004, *Mar. Geod.*, *29*, 149–166, doi:10.1080/01490410600939140.

Ito, Y., T. Matsumoto, H. Kimura, H. Matsubayashi, K. Obara, and S. Sekiguchi (2005), Spatial distribution of centroid moment tensor solutions for the 2004 off Kii peninsula earthquakes, *Earth Planets Space*, *57*, 351–356.

Kajiura, K. (1963), The leading wave of a tsunami, *Bull. Earthquake Res. Institute*, *41*, 545–571.

Kanamori, H. (1972), Mechanism of tsunami earthquake, *Phys. Earth Planet. Inter.*, *6*, 246–259, doi:10.1016/0031-9201(72)90058-1.

Kanamori, H., and D. L. Anderson (1975), Theoretical basis of some empirical relations in seismology, *Bull. Seismol. Soc. Am.*, *65*, 1073–1095.

Kato, T., Y. Terada, M. Kinoshita, H. Kakimoto, H. Isshiki, M. Matsuishi, A. Yokoyama, and T. Tanno (2000), Real-time observation of tsunami by RTK-GPS, *Earth Planets Space*, *52*, 841–845.

Matsumoto, H., and H. Mikada (2005), Fault geometry of the 2004 off the Kii peninsula earthquake inferred from offshore pressure waveforms, *Earth Planets Space*, *57*, 161–166.

Miyoshi, T., and K. Ishibashi (2005), A tectonic interpretation of NW-SE strike-slip faulting during the 2004 off the Kii peninsula earthquakes, Japan: Probable tear of the Philippine Sea plate, *Earth Planets Space*, *57*, 1115–1120.

Obara, K. (2009), Inhomogeneous distribution of deep slow earthquake activity along the strike of the subducting Philippine Sea Plate, *Gondwana Res.*, *16*, 512–526, doi:10.1016/j.gr.2009.04.011.

Okada, Y. (1985), Surface deformation due to shear and tensile faults in a half space, *Bull. Seismol. Soc. Am.*, *75*, 1135–1154.

Park, S.-C., and J. Mori (2005), The 2004 sequence of triggered earthquakes off the Kii peninsula, Japan, *Earth Planets Space*, *57*, 315–320.

Peregrine, H. (1972), Equations for water waves and the approximations behind them, edited by R. E. Meyer, pp. 95–121, *Waves on Beaches and Resulting Sediment Transport*, Academic Press, New York.

Piatanesi, A., and S. Lorito (2007), Rupture process of the 2004 Sumatra-Andaman Earthquake from Tsunami waveform inversion, *Bull. Seismol. Soc. Am.*, *97*, S223–S231, doi:10.1785/0120050627.

Press, W. H., B. P. Flannery, S. A. Teukolsky, and W. T. Vetterling (1986), *Numerical Recipes*, Cambridge Univ. Press, Cambridge.

Saito, T., and T. Furumura (2009a), Three-dimensional simulation of tsunami generation and propagation: Application to intraplate events, *J. Geophys. Res.*, *114*, B02307, doi:10.1029/2007JB005523.

Saito, T., and T. Furumura (2009b), Three-dimensional tsunami generation simulation due to sea-bottom deformation and its interpretation based on the linear theory, *Geophys. J. Int.*, doi:10.1111/j.1365-246X.2009.04206.x.

Satake, K. (1989), Inversion of tsunami waveforms for the estimation of heterogeneous fault motion of large submarine earthquakes: The 1968 Tokachi-oki and 1983 Japan Sea earthquakes, *J. Geophys. Res.*, *94*, 5627–5636, doi:10.1029/JB094iB05p05627.

Satake, K., T. Baba, K. Hirata, S. Iwasaki, T. Kato, S. Koshimura, J. Takenaka, and Y. Terada (2005), Tsunami source of the 2004 off the Kii Peninsula earthquakes inferred from offshore tsunami and coastal tide gauges, *Earth Planets Space*, *57*, 173–178.

Shigihara, Y., and K. Fujima (2006), Wave dispersion effect in the Indian Ocean tsunami, *Journal of Disaster Research*, *1*, 142–147.

Shiomi, K., and J. Park (2008), Structural features of the subducting slab beneath the Kii Peninsula, central Japan: Seismic evidence of slab segmentation, dehydration, and anisotropy, *J. Geophys. Res.*, *113*, B10318, doi:10.1029/2007JB005535.

Takahashi, R. (1942), On seismic sea waves caused by deformations of the sea bottom, *Bull. Earthq. Res. Inst.*, *20*, 357–400 (in Japanese with English abstract).

Tanioka, Y. (2000), Numerical simulation of far-field tsunamis using the linear Boussinesq equation-—The 1998 Papua New Guinea tsunami, *Pap. Meteorol. Geophys.*, *51*, 17–25, doi:10.2467/mripapers.51.17.

Tsushima, H., R. Hino, H. Fujimoto, Y. Tanioka, and F. Imamura (2009), Near-field tsunami forecasting from cabled ocean bottom pressure data, *J. Geophys. Res.*, *114*, B06309, doi:10.1029/2008JB005988.

Wessel, P., and W. H. F. Smith (1998), New improved version of generic mapping tools released, *Eos Trans. AGU*, *79*, 579.

T. Furumura and K. Satake, Earthquake Research Institute, University of Tokyo, Tokyo, 1-1-1 Yayoi, Bunkyo-ku 113-0032, Japan.

T. Saito, National Research Institute for Earth Science and Disaster Prevention, 3-1 Tennodai, Tsukuba, Ibaraki 305-0006, Japan. (saito-ta@bosai.go.jp)